BIOCHEMISTRY
including biophysical chemistry & molecular biology

Article

pubs.acs.org/biochemistry

Multiple Structural States Exist Throughout the Helical Nucleation Sequence of the Intrinsically Disordered Protein Stathmin, As Reported by Electron Paramagnetic Resonance Spectroscopy

Ashley J. Chui,[†,§] Carlos J. López,[‡,§] Evan K. Brooks,[‡] Katherina C. Chua,[†] Tonia G. Doupey,[†] Gretchen N. Foltz,[†] Joseph G. Kamel,[†] Estefania Larrosa,[†] Amissi Sadiki,[†] and Michael D. Bridges*[,†,§]

[†]Department of Chemistry and Biochemistry, California State University Fullerton, Fullerton, California 92831-6866, United States

[‡]Department of Chemistry and Biochemistry and the Jules Stein Eye Institute, University of California, Los Angeles, California 90095-7008, United States

Supporting Information

ABSTRACT: The intrinsically disordered protein (IDP) stathmin plays an important regulatory role in cytoskeletal maintenance through its helical binding to tubulin and microtubules. However, it lacks a stable fold in the absence of its binding partner. Although stathmin has been a focus of research over the past two decades, the solution-phase conformational dynamics of this IDP are poorly understood. It has been reported that stathmin is purely monomeric in solution and that it bears a short helical region of persistent foldedness, which may act to nucleate helical folding in the C-terminal direction. Here we report a comprehensive study of the structural equilibria local to this region in stathmin that contradicts these two claims. Using the technique of electron paramagnetic resonance (EPR) spectroscopy on spin-labeled stathmin mutants in the solution-phase and when immobilized on Sepharose solid support, we show that all sites in the helical nucleation region of stathmin exhibit multiple spectral components that correspond to dynamic states of differing mobilities and stabilities. Importantly, a state with relatively low mobility dominates each spectrum with an average population greater than 50%, which we suggest corresponds to an oligomerized state of the protein. This is in contrast to a less populated, more mobile state, which likely represents a helically folded monomeric state of stathmin, and a highly mobile state, which we propose is the random coil conformer of the protein. Our interpretation of the EPR data is confirmed by further characterization of the protein using the techniques of native and SDS PAGE, gel filtration chromatography, and multiangle and dynamic light scattering, all of which show the presence of oligomeric stathmin in solution. Collectively, these data suggest that stathmin exists in a diverse equilibrium of states throughout the purported helical nucleation region and that this IDP exhibits a propensity toward oligomerization.

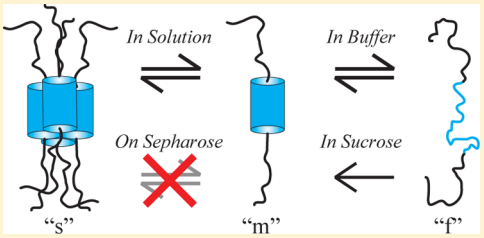

Intrinsically disordered proteins (IDPs) are an interesting class of biomolecules that are estimated to constitute ca. 30% of eukaryotic genomes[1−3] and which lack a native and stable three-dimensional fold under physiological conditions. Although some IDPs are toxic or pathogenic (e.g., some forms of α-synuclein and amyloid-β), many of these highly flexible, unstructured proteins play important roles in cellular signaling and metabolic regulation.[4] Since their discovery, IDPs have helped to reveal the strong link between protein flexibility and biological functionality, with "coupled folding and binding'" being a central theme in discussions of regulatory IDP behavior.[5,6] Because of their innate instability, which stems from the relative magnitude of energy fluctuations inherent to biologically relevant temperatures,[7] these highly dynamic proteins typically explore a variety of conformations as monomers or, in some cases, adopt a lowest energy state as an oligomer or aggregate.[8,9]

Stathmin, the primary member in a family of "stathmin-like" IDPs, is a ubiquitous cytoplasmic protein found in eukaryotic cells and is part of a signaling pathway to regulate cell proliferation, differentiation, and function by controlling microtubule growth. Its disregulation has also been directly linked to abnormal cell behavior and the proliferation of cancer tissue.[10] Stathmin is a 17 kDa, 149-residue protein suggested to exist in solution in a structural equilibrium of a flexible, extended α-helix (~90 residues long) and various less-structured random coil configurations.[11,12] The N-terminal region of the protein (residues 1−40) does not exhibit any secondary structure other than a β-hairpin from residues 7−23, though it acts as a capping domain (Figure 1A) when stathmin is bound to tubulin, the protein subunit that polymerizes into microtubules. The remainder of the protein, residues 41−149, is termed the "C-terminal helix", and in the tubulin-stathmin binding complex (referred to as the "T_2S" heteropentamer) this region is tightly bound to two $\alpha\beta$-tubulin heterodimer subunits.

A substantial portion of the C-terminal helix sequence (residues 48−118) contains approximately eight distinct heptad

Received: July 20, 2014
Revised: February 23, 2015
Published: February 25, 2015

DOI: 10.1021/bi500894q
Biochemistry 2015, 54, 1717−1728

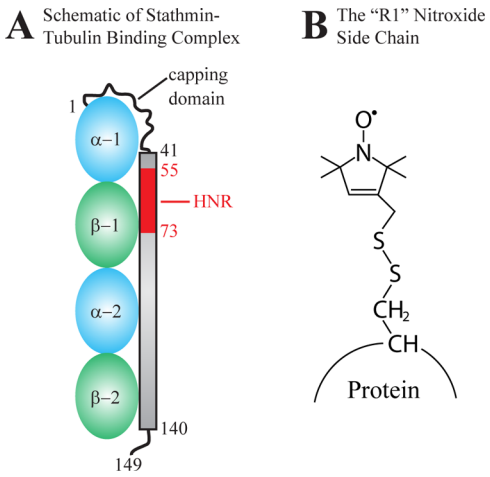

Figure 1. Stathmin and the R1 side chain. (A) Schematic of the stathmin-tubulin "T2S" binding complex, which indicates the approximate locations of the disordered N-terminal capping domain (residues 1−40) and the C-terminal helix (residues 41−140 in gray) wherein the helical nucleation region lies ("HNR" - residues 55−73 in red). (B) The "R1" nitroxide side chain often used in protein backbone dynamics studies by SDSL EPR.

repeats,[13] suggesting that stathmin could have a propensity to form coiled-coil oligomers. However, analytical ultracentrifugation studies of stathmin at 4 and 20 °C, revealed an average molecular weight consistent with that of a monomer, contradicting the prediction of a coiled-coil.[14] The same study also revealed a temperature-dependent elongated shape in the protein that could be interpreted as evidence of a fleetingly stable α-helix.

Residues 55−73 in the C-terminal helix comprise a primary area of interest in solution phase stathmin, which here we call the "helical nucleation region" (HNR), an adaptation of the two monikers "helix initiation site"[14] and "major helix nucleation site"[12] given by Steinmetz et al. On the basis of the dynamics and relative stability of this section of the protein, it appears to play a central role in driving further helical folding in the C-terminal direction upon binding. Far-UV circular dichroism (CD) spectroscopy studies[11] on various deletion mutants indicate that solution-phase stathmin is approximately 60% helical over its full length at 5 °C, which decreases to 40% helicity at 25 °C. At this temperature, the HNR is reported to be predominantly folded, though increasing temperatures to 40 °C induces a noncooperative transition from a helix to a mostly denatured state, a transition that is fully reversible. It is important to note that Steinmetz et al.[12] also report rapid exchange between helical and random coil conformations throughout the entire C-terminal helix region of stathmin by 2D-NMR at 25 °C. This observation contradicts the existence of the HNR as a segment of arbitrarily high helical stability and is a result that is possibly more biologically relevant, as it summarizes the behavior of an untruncated intrinsically disordered protein in near-physiological conditions.

We suspect that the above three techniques are insensitive to some aspects of the actual behavior of the stathmin molecule in solution. High hydrostatic pressures created by analytical ultracentrifugation can cause the dissociation of loosely bound oligomers,[15,16] CD spectroscopy reports an ensemble average of protein structure and thus cannot deconvolute the individual components of any equilibria that may exist, and NMR spectroscopy cannot separate or quantitatively characterize multiple structural states in conformational exchange on the long-nanosecond to microsecond time scales.[7] In contrast, the technique of site-directed spin-labeling (SDSL) combined with electron paramagnetic resonance (EPR) spectroscopy is able to characterize and quantify multiple structural components in proteins under physiological conditions with site-specific resolution,[17−19] and it can indicate situations of oligomerization or aggregation in spin-labeled proteins as spectral line broadening arising from the dipolar interaction.[20] Complementary techniques such as native polyacrylamide gel electrophoresis (PAGE), gel filtration chromatography, and dynamic light scattering (DLS) are ideally suited to confirm the existence of, and further characterize, any oligomers present in solution; a portion of the study reported herein employs these tools to investigate the existence of oligomeric states of stathmin.

A small number of IDPs have been studied by SDSL EPR; for a comprehensive review, see Drescher (2012).[21] The IDP-EPR literature is primarily dominated by research on α-synuclein,[22,23] found in the Lewy bodies of patients with Parkinson's disease, and amyloid-β peptide,[24−26] the key component in the amyloid plaques of Alzheimer's disease. SDSL EPR was particularly successful in revealing the various structural states and higher-order organizations of these proteins in their various oligomerized and aggregated forms. Other reported SDSL EPR studies on IDPs also include those of prion protein H1,[27] ubiquitin,[28] and the disordered region of measles virus nucleoprotein.[29] As is commented by Drescher,[21] because of its marginal perturbation of IDP structure and its ability to probe an isolated, local protein environment, SDSL EPR is an effective tool in the investigation of IDP structure and dynamics.

In this study we investigated whether the putative HNR region adopts a stable helical structure or an ensemble of alternative conformations that exist on a time scale distinguishable within the EPR detection-window by analyzing the room temperature continuous wave (CW) EPR spectra for stathmin mutants that are spin-labeled at sites within the HNR (residues 52−76) in the solution phase and immobilized on Sepharose beads. CD spectroscopy for a set of representative spin-labeled mutants was performed to investigate the structural integrity and relative stabilities of these modified proteins. The CD data reveal that the addition of the nitroxide spin label in this region has little effect on the secondary structure and stability of stathmin compared to the wild type (WT) analogue, while the CW EPR data suggest that the HNR region of stathmin exists in an equilibrium between multiple states, one of which may correspond to an oligomeric state. Indeed, here we confirm oligomeric states of stathmin by native and sodium dodecyl sulfate (SDS) PAGE, gel filtration chromatography, multiangle light scattering (MALS), DLS, and dipolar broadening EPR. While it has been suggested that stathmin is a pure monomer in solution and that its HNR exists in a state of persistent foldedness (i.e., it is kinetically trapped in a folded state[11,12]), the findings herein unequivocally show that soluble stathmin explores a monomer−oligomer equilibrium and that the HNR region in the monomeric protein fluctuates between at least two structural states.

EXPERIMENTAL PROCEDURES

Site-Directed Mutagenesis. Plasmid vector pET-15b (Novagen), containing ampicillin resistance and T7 promoter and terminator sites, was modified such that it contained the gene for a fusion protein containing wild-type human stathmin ("STMN1", available from Invitrogen in a pDNR-LIB vector). The fusion construct gene (a generous gift from Dr. David

DOI: 10.1021/bi500894q
Biochemistry 2015, 54, 1717−1728

Eisenberg, University of California, Los Angeles) consisted of a poly-histidine sequence tag (His_6), maltose binding protein (MBP), and a tobacco etch virus protease (TEV)-specific cut site (sequence ENLYFQG), to which wild-type (WT) human stathmin with its ATG start codon removed was ligated.

Positions for cysteine mutation (for spin-labeling) were inclusive of the range K52 to R76, and primers were designed for compatibility with the QuikChange II (Agilent Technologies, Santa Clara, CA) polymerase chain reaction (PCR) protocol, which was followed. Lysine-to-alanine mutants (K52A, K53A, K52A/K53A, and K70A) were prepared by the same method. PCR product DNA was transformed into NEB 5-alpha competent cells (New England Biolabs, Ipswich, MA), plated on Luria−Bertani (LB) agar plates containing 0.1 g/L ampicillin, and incubated overnight at 37 °C. Overnight cultures in 20 mL of LB media with 0.1 g/L ampicillin added were prepared, and DNA was purified from the resulting pellets using the QIAprep Spin Miniprep kit (Germantown, MD) for mutant sequence verification (GENEWIZ Inc., South Plainfield, NJ).

Expression and Purification of Stathmin. Wild-type protein and cysteine mutants of stathmin were transformed into competent BL21(DE3) cells (New England Biolabs, Ipswich, MA), plated on LB agar plates containing 0.1 g/L ampicillin, and incubated overnight at 37 °C. From these plates, 25 mL starter cultures were grown overnight at 37 °C, followed by further growth in 1 L of LB media with 0.1 g/L ampicillin with shaking at 37 °C for approximately 4 h. Expression of the stathmin fusion construct was then induced with isopropyl β-D-1-thiogalactopyranoside (0.234 g/L), and incubation-shaking was continued as before another 2−3 h. Cells were immediately harvested by centrifugation at 6000 rpm for 15 min, and the pellet was resuspended in 34 mL of buffer A1 (50 mM potassium phosphate, 100 mM NaCl, 0.5 g/L dithiothreitol (DTT), pH 7.4). Prior to lysis, the protease inhibitors phenylmethylsulfonyl fluoride, leupeptin, pepstatin, and aprotinin (each to 1 mM) were added to the resuspended cell pellets. Cells were lysed by sonication, the resulting solution was centrifuged at 45000*g* for 30 min, and then the supernatant was filtered through 0.45 and 0.20 μm PES syringe filters.

The fusion protein was purified by fast protein liquid affinity chromatography using a HisTrap FF column (GE Healthcare) and detected at an absorbance of 280 nm. An imidazole gradient was used to elute the His_6-MBP-cut-STMN construct from the column by blending buffer A1 and buffer A2 (50 mM potassium phosphate, 500 mM NaCl, 0.5 g/L dithiothreitol (DTT), 500 mM imidazole, pH 7.4). After an initial rinse of the column with 4% buffer A2 to remove nonspecifically bound proteins, the fusion construct eluted between 30 and 50% A2 depending on the mutant. Active TEV protease (~200 μg), which was prepared according to the method of Laganowsky et al.[30] (the plasmid containing the gene for TEV expression was a generous gift from Dr. Wayne Hubbell, University of California, Los Angeles), was added to the fusion protein eluted fraction, and this solution was dialyzed overnight in 50 times its volume of A1, with the purpose of cleaving stathmin from the rest of the construct while removing trace imidazole. Free stathmin was purified from the His_6-MBP fragment by HisTrap FF Nickel-affinity chromatography as above, except that absorbance detection was set to 230 nm (WT stathmin does not absorb at 280 nm) and that stathmin—no longer bearing a His_6-tag—does not bind to the column and is thus found in the flow-through fraction.

Spin-Labeling of Stathmin. Purified stathmin fractions were concentrated in Amicon Ultra-4 Centrifugal Filter Units (EMD Millipore, Billerica, MA) to a working volume of 10 mL and were then washed via a HiPrep 26/10 desalting column (GE Healthcare) equilibrated with "spin-labeling buffer" (50 mM MOPS, 25 mM NaCl, pH 6.8) to remove DTT and imidazole, and with absorbance detection at 230 nm. 10-fold molar excess of the R1 nitroxide spin label reagent (1-oxy-2,2,5,5,-tetramethyl-pyrrolin-3-methylmethanethiosulfonate spin label, MTSSL or HO-225) in acetonitrile was immediately added to the stathmin fraction and allowed to react on a nutator at room temperature for at least 30 min; excess spin label was then removed by a second wash via the desalting column, as described above. Spin-labeling efficiency for all spin-labeled mutants studied was quantified to be in the range of 85−100% using the Measure-iT Thiol Assay Kit (Life Technologies). Wild-type and spin-labeled mutant solutions of stathmin were then quantified using a bicinchoninic acid protein assay kit (Pierce Biotechnology, Rockford, IL).

Covalent Attachment of Stathmin to Sepharose. CNBr-activated Sepharose 4B (GE Healthcare) was suspended and washed with multiple 100 mL aliquots of 1 mM HCl (pH 2.0) for 15 min, and the HCl was removed with the same volume of spin-labeling buffer over 15 min. Any trace solids present in the spin-labeled protein solutions were first removed by centrifugation, and the protein concentrations were adjusted to final values within the range of 100−250 μM, which were added to the Sepharose beads in a 2:1 protein solution/Sepharose volume ratio. The coupling reaction was mixed on a nutating platform at room temperature for at least 1 h, or at 4 °C overnight. Uncoupled protein was then removed with multiple rinses of spin-labeling buffer.

Sample Preparation for Basic CW-EPR. Following spin-labeling and a final desalting run, solution-phase ("buffer") protein samples were concentrated to a working range of 100−250 μM. Protein mutants covalently attached to Sepharose solid support were equilibrated with either spin-labeling buffer or sucrose-buffer (at a concentration of 5, 10, 15, 20, 25, or 30% w/w in spin-labeling buffer) via multiple rinses with the appropriate solution. Samples were loaded into quartz capillary tubes (0.60/0.84 × 100 mm; Vitrocom Inc., Mountain Lakes, NJ) via capillary action; tubes were sealed at both ends with Critoseal (Leica Microsystems, Buffalo Grove, IL).

Sample Preparation for Dipolar-Broadening CW-EPR. Dipolar broadening EPR studies often involve the spectral comparison of two different sample types: a pure solution of a particular spin-labeled mutant (where dipolar broadening due to oligomerization/aggregation would be maximal), and a solution that is a mixture of WT and spin-labeled mutant stathmin (which we term a "wild-type dilution", where spectral line broadening is decreased due to a reduction in the number of spin labels per oligomer). For this study, wild-type stathmin and a spin-labeled stathmin mutant (K53R1 or L72R1) solutions were mixed in a 5:1 mol ratio, respectively, and this mixture was then diluted to a total protein concentration of 300 μM using spin-labeling buffer. "Pure spin-labeled protein" and "wild-type diluted" solutions were then attached to Sepharose beads and loaded into quartz capillaries as described above.

CW-EPR Spectroscopy. The continuous wave EPR spectra were recorded on a EMXplus X-band spectrometer (Bruker BioSpin Corporation, Billerica, MA) with a scan width of 100 G, modulation amplitude of 1 G, and an incident microwave power of 20 mW. All spectra were obtained at the ambient temperature of a climate-controlled room (which ranged from 19.5 to 22.5 °C). Prior to analysis, the integrated areas of all EPR spectra were

DOI: 10.1021/bi500894q
Biochemistry 2015, 54, 1717−1728

normalized such that their line shapes are directly comparable, regardless of relative concentration.

Circular Dichroism Spectroscopy, EPR Spectral Simulations, Native and SDS PAGE, Gel Filtration Chromatography, and Multiangle and Dynamic Light Scattering. Detailed descriptions of the full experimental procedures for circular dichroism spectroscopy, EPR spectral simulations, native and SDS PAGE, gel filtration chromatography, and multiangle and dynamic light scattering can be found in the Supporting Information.

RESULTS AND DISCUSSION

Experimental Strategy To Study the Conformational Flexibility and Structural States of Stathmin in Solution via SDSL-EPR. In SDSL, a neutral, stable nitroxide free radical is covalently attached to a protein in a region of interest; this is done through the introduction of a cysteine mutation at an amino acid site in that region and then by reaction of the mutant with a sulfhydryl-selective methanethiosulfonate spin-labeling reagent. The nitroxide reagent of most widespread use is (1-oxyl-2,2,5,5-tetramethylpyrroline-3-methyl) methanethiosulfonate, which generates the EPR-active side chain that we commonly designate as "R1" at the site of interest (Figure 1B). To avoid protein destabilization by this process, solvent-exposed sites are typically chosen for spin-labeling studies. Stathmin, particularly in the HNR, is assumed to exist as a long α-helix or random coil in solution, and so all sites we selected for spin labeling in this study (52−76) are expected to be solvent-exposed if the protein is monomeric. At such sites, the X-band EPR spectra of R1-labeled proteins directly reveal the motion of the nitroxide side chain and backbone fluctuations in the picosecond to nanosecond time scale.[17,19,31] The motion of R1 within this time scale has been shown to be primarily determined by the local environment[32,33] and the intrinsic flexibility of the backbone.[19,31] The relative rates and amplitudes of motion in the picosecond to nanosecond time scale can be conveniently obtained using a popular spectral simulation program[34] that utilizes the stochastic Liouville motional model of Freed and Budil.[35] On the other hand, spin-labeled sites located in regions that exchange between multiple structural states on the time scale of microseconds (μs) or longer—a common occurrence[17−19,31−33,36]—will exhibit multi-component (or "complex") EPR spectra. Usually, such spectra can be easily separated into individual components via simulation, and each modeled component can be characterized and quantified to describe the existing dynamic states at equilibrium. Thorough reviews of the methodologies of SDSL EPR are available.[18,37,38]

In situations of protein oligomerization or aggregation, EPR spectroscopy can reveal the existence of higher order complexes if spin labels on different the polypeptide chains in the complex are close enough to one another (<25 Å) to show broadening of the spectral line shape due to the dipolar interaction.[20] In this study, CW line shape analysis of R1 sites throughout the helical nucleation region was done to study fast backbone dynamics, identify regions in exchange, and investigate whether oligomeric states of stathmin exist in solution.

The R1 Nitroxide Side Chain Has Negligible Effect on the Secondary Structure and Thermal Stability of Stathmin. To determine the structural and thermodynamic effects of site-directed spin-labeling on the helical nucleation region of stathmin, spin-labeled mutants at six representative sites were studied by thermal unfolding and far-UV circular dichroism spectroscopy (Figure 2).

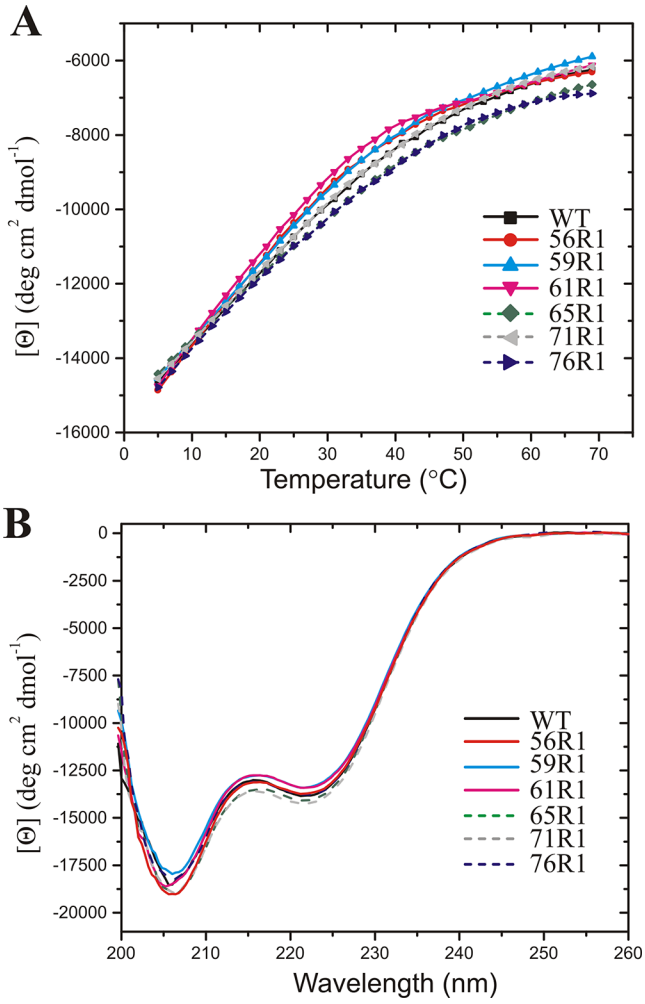

Figure 2. Thermal Unfolding and far-UV CD traces for WT and representative R1-labeled stathmin mutants. (A) Thermal unfolding profiles. (B) Far-UV CD profiles at 5 °C. Note the very minor differences between WT and mutant traces, indicating a negligible effect of spin-labeling on stathmin stability.

For the thermal unfolding of WT and R1 mutants, a broad unfolding transition with no pretransition baseline is evident (Figure 2A), which is indicative of noncooperative unfolding and a lack of stable tertiary structure (whereas a protein with stable tertiary structure would exhibit a sigmoidal unfolding curve). For all mutants investigated, thermal unfolding was fully reversible, and the unfolding curve of WT was similar to that shown in Honnoppa et al.[11] Since the thermal denaturation of stathmin showed no pretransition baseline and the unfolding is not a two-state process, true thermodynamic parameters (T_m, ΔG, ΔH_m) cannot be extracted. Qualitatively, the unfolding profiles of the six R1 mutants studied were similar to that of WT protein, showing a minor overall shift to lower temperatures (up to 3 °C for 61R1), which is indicative of a very minor destabilization relative to the WT. The small degree of destabilization in stathmin attributed here to mutagenesis and spin-labeling is well within the range observed for R1 mutants at surface sites in various stable and well-ordered proteins.[17,32]

The far-UV CD profiles for WT and R1 mutants show two minima centered at 207 and 222 nm (Figure 2B). The subtle differences in the mean residue ellipticity between the WT protein and the R1 mutants (less than 5% throughout the range)

DOI: 10.1021/bi500894q
Biochemistry 2015, 54, 1717−1728

suggest that, for the six mutants investigated, the introduction of R1 has little effect on the secondary structure of stathmin. On the basis of this and the thermal denaturation results above, we are confident that introduction of the nitroxide spin label to various sites within the HNR of stathmin has a negligible effect on the stability and native structural equilibria of the protein.

Experimental Considerations for EPR Spectral Analysis of Stathmin Mutants in Solution and Immobilized on Solid Support. To study the molecular flexibility and dynamics of stathmin in and around its putative HNR, sites 52 through 76 were spin-labeled, and the X-band EPR spectra were recorded at room temperature. At X-band frequency, the continuous wave (CW) EPR technique is sensitive to the overall rotational diffusion of small proteins ($M_r \leq 50$ kDa) like stathmin and, as such, solution-phase EPR spectra will have dramatic line shape contributions from the rapid tumbling. In order to eliminate the effect of this rotational diffusion and resolve internal protein backbone modes, a common strategy employed in CW EPR experiments involves addition of viscosity agents[17,39,40] or total immobilization of the protein on solid surfaces by covalent attachment.[41−43] In this portion of the study, we report the EPR spectra of spin-labeled stathmin in three environments: in the solution phase (pure buffer), in buffer containing 30% w/w sucrose, and covalently tethered to a solid support (CNBr-Sepharose). For SDSL applications, covalent attachment of spin-labeled protein via lysine residues to CNBr-activated Sepharose has been shown to effectively slow overall protein tumbling to a rotational diffusion time scale >50 μs,[44] thus enabling quantitative analysis of internal protein modes without any contribution from tumbling. However, a disadvantage of the tethering strategy employed here is the random orientation of the protein relative to the matrix, which can give rise to a small population of immobile states due to R1-matrix interaction in cases where the attachment occurs via lysine residues near the R1 side chain.[43] There are 23 lysines in stathmin (Figure S1, Supporting Information); five are within or close to the HNR, and so EPR spectra for spin-labeled stathmin may exhibit relatively immobile components as a result of Sepharose-attachment. However, in the cases investigated we found that the EPR spectra for variants where alanine was used to replace lysine residues close to spin-labeling sites in the HNR were only slightly different from those seen in the WT background (Figures S2, S3 and S4, Table S1, and associated text), and thus we are confident that the qualitative features of the EPR spectra obtained for Sepharose-bound spin-labeled stathmin mutants are also relevant to solution-phase stathmin. For comparison, the results for the spectra acquired for solution-phase stathmin mutants in buffer and in sucrose are discussed.

Spin-Labeled Stathmin Sites in the Putative Helix Nucleation Region Exhibit Multicomponent EPR Spectra Indicative of Multiple States of Varying Mobility and Order. Figure 3 shows EPR spectra and simulations for representative spin-labeled sites within the HNR of stathmin tethered to CNBr-Sepharose (EPR spectra and simulations for all 25 sites in this region, 52R1 through 76R1, are provided in Figure S5). Qualitatively, all EPR spectra throughout the HNR sequence exhibit multiple motional components; one of these components has a relatively sharp line shape indicating a state of high nitroxide side chain mobility. To determine relative population, rotational correlation time, and amplitude of nitroxide motion for each spectral component, spectral simulations (i.e., fits to the data) were obtained. A detailed description of the strategy for spectral simulations can be found

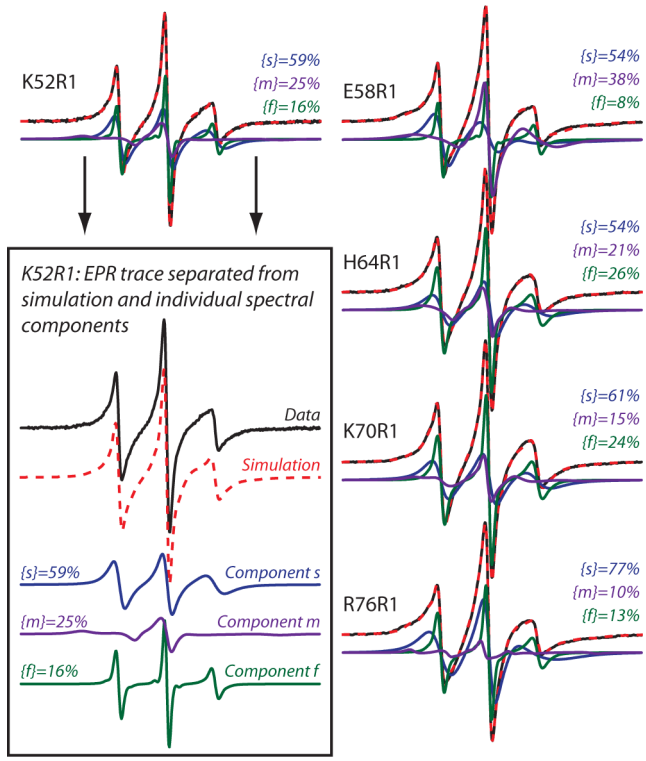

Figure 3. EPR spectra and spectral-fitting simulations for representative spin-labeled stathmin mutants at sites in and around the HNR. Data (black traces) were acquired for protein covalently attached to Sepharose in a buffer environment; all scans are 100 G wide. Each simulation (red dashed traces) required three spectral components for satisfactory fits to the data, which were categorized as nitroxide states with differing dynamic properties: "s", immobile and nonpolar (blue traces); "m", moderate mobility and polar (purple traces); "f", high mobility and polar (green traces). See Figure S5 for EPR spectra and simulations of all 25 Sepharose-attached mutants in and around the HNR; dynamic parameters used to produce each spectral simulation are given in Table S2 of the Supporting Information and average values are given in Table 1.

in the Supporting Information. All mutants attached to CNBr-Sepharose require simulations comprised of three separate spectral components that we have labeled "s", "m", and "f" (average dynamic parameters used in simulations are given in Table 1), as attempts using only one or two components yielded unsatisfactory fit quality. Each spectrum is dominated by a relatively immobile state ("s") with relative populations ranging from 42 to 77% (see Table S2 for the simulation parameters used to fit to each individual spectrum shown in Figures 3 and S5). Simulations of this component report no nitroxide ordering potential ($S = 0$), a long average rotational correlation time of ca. 15 ns (i.e., a state of very low mobility), and a nonpolar local environment as judged by relatively small hyperfine splitting values ($A_{zz} = 34-36$ G; see the SI for a discussion of the relevant fitting parameters reported here). Reasonable fits were only obtained by using a large Lorentzian line width parameter for the majority of mutants studied ($w_{bar} = 2$ G), likely indicating local structural heterogeneity, dipolar broadening, or both.

The relative population of the second component (m) varied from 6 to 38% and exhibited moderate mobility with an average rotational correlation time of $\tau_R \approx 5$ ns and a moderate ordering potential in the range of $S = 0.08-0.55$. It is noted that relatively large hyperfine splitting values were required for this component

DOI: 10.1021/bi500894q
Biochemistry 2015, 54, 1717−1728

Table 1. Summarized Principal Simulation Parameters Obtained for the Different Three Components Observed in Sepharose-Attached Stathmin Mutants in a Buffer Environment[a]

spectral component	mobility and environment	τ_R (ns)	S	A_{zz} (G)	w_{bar} (G)	population (%)	solution-phase population (%)[c]
s	immobile/nonpolar	15(2)	0[b]	35.4(6)	1.7(6)	56(7)	{s} + {m} = 77(8)
m	moderate/polar	5.1(8)	0.3(1)	38.5(3)	0.9(2)	23(8)	
f	mobile/polar	2.1(5)	0[b]	38.9(6)	0.3(1)	21(9)	{f} = 23(9)

[a]Fitting parameters for all individual mutants provided in the Supplementary Information. Parameter set standard deviations in the last digit shown are given in parentheses. [b]The order parameter, S, was fixed to zero during simulation of the "s" and "f" components, as this variable would automatically migrate toward zero for these components when unfixed. [c]Component populations for the two states observed in the solution phase (i.e., stathmin not tethered to Sepharose) is also provided here. We suggest that the lower mobility spectral component seen in the solution phase corresponds to the "s" and "m" states seen in Sepharose-attached mutants, which are spectrally merged due to rapid rotational tumbling.

(A_{zz} = 37−39 G) suggesting a polar environment local to the R1 side chain. Upon first examination, comparison of the spectral line shapes for components "s" and "m" may cause confusion, as the faster-tumbling (m) component exhibits a wider spectrum with slightly broader lines. It is worthwhile to mention, however, that the line shapes simulated are products of not only the rotational correlation time, but also the order parameter (zero for "s", nonzero for "m"), A_{zz} (where different local polarities will result in different line splittings), and w_{bar} (largest for "s" as we suspect dipolar broadening, structural heterogeneity, or both for this state).

The third spectral component (f) seen in each spectrum (8−52% population) reflects isotropic motion (S = 0) of high mobility of R1 ($\tau_R \approx 2$ ns) similar to those observed in highly flexible protein sequences.[19] Reasonable fits were obtained using small Lorentzian line width broadening parameters for fitting the "m" and "s" components ($w_{bar} \leq 1$ G), which suggest structural homogeneity in these states.

It is interesting to note that by excluding the simulation parameters obtained for mutant S63R1, the individual population ranges for all three components narrow (to s = 49−77%, m = 10−38%, and f = 8−32%). We suspect that this spin-labeled mutant exhibits such different simulation parameters because of the functional nature of site S63 itself, namely, that phosphorylation of this serine residue dramatically reduces the stability of the HNR.[12] Spin-labeling at residue 63, while not producing an anionic side chain at the site, does increase the local bulk and polarity; it is possible that this emulates phosphorylation in part and thus destabilizes the region.

Spectral analysis for stathmin mutants in a solution-phase buffer environment yields only two distinct motional components (see Figure S6 and Table S3), with a dominant population of low mobility, low order, and high spectral inhomogeneity, and a smaller population of a high mobility, zero order state. It is likely that the high population, low-mobility spectral component seen in these buffer-phase spectra is, in fact, representative of the two lower-mobility states seen when stathmin is attached to solid support (i.e., states "s" and "m"), which have spectrally merged due to fast rotational diffusion of the protein in buffer. Of relevance here is that the fitted population of the high-mobility component is essentially identical in both environments (see the rightmost column of Table 1), suggesting that covalent attachment to Sepharose does not shift the relative populations of coexisting dynamic states in this protein.

Addition of Sucrose to Sepharose-Tethered Stathmin Reveals That Two of the Conformational States Observed in the HNR Are in Equilibrium. As discussed above, SDSL experiments often employ viscogens, such as sucrose, to minimize the large contribution of rotational diffusion in X-band EPR spectra.[39,40] However, as a "protecting osmolyte", sucrose is also known to drive protein conformational equilibria toward states in which the peptide backbone has the lowest possible exposure to water.[45,46] For this reason, this effect can be used to distinguish rotameric from conformational exchange processes, both of which show up as multicomponent EPR spectra.[41] For globular proteins, the addition of sucrose typically results in an equilibrium shift toward the most folded protein state; however, in IDPs it is unclear if the addition of sucrose will generally result in a folded (or "bound-like") state[47] or if it would instead populate a disordered aggregate resulting from the coalescence of many random coil molecules. Alternatively, for IDPs prone to oligomerization, it is possible that the addition of a protecting osmolyte could stabilize the most oligomerized state of the protein.[48] To explore whether the distribution of conformational states seen in the HNR of stathmin on Sepharose truly reflect equilibrium between multiple conformational states, the effect of sucrose on component populations was investigated by CW EPR. It is noted that this strategy has already been successfully applied in various SDSL studies.[41,49,50]

We observed that EPR spectra recorded for solution-phase stathmin in a sucrose environment are broader than those observed for Sepharose-tethered stathmin (compare the black traces in Figures S2 and S4). This likely reflects changes in the conformational flexibility of stathmin due to the presence of the added sucrose. Sixteen representative spin-labeled mutants tethered to Sepharose were studied in pure buffer and in the presence of 30% w/w sucrose (∼1 M concentration). Figure 4 shows the spectra for six representative mutants; the entire set is given in Figure S7 along with Table S4 which provides the dynamic parameters obtained from simulation. Qualitatively, we note that the addition of sucrose causes the apparent depopulation of the sharpest ("f") spectral component while transferring this population to the moderate mobility ("m") state, and leaving the "s" component relatively unaffected.

Note that, since Sepharose-bound stathmin is completely immobilized, the spectral changes that occur following the addition of sucrose cannot arise from reduction in overall tumbling rate or from aggregation, but rather comes from changes in the local protein structure;[41] thus the noticeable disappearance of the high mobility "f" component is a clear indication of changes in the conformational equilibrium of the HNR in stathmin. This observation was quantitatively verified through simulations of the spectra for Sepharose-attached stathmin mutants in sucrose. Reasonable fits were obtained by increasing the population of the "m" state with a concomitant decrease of the "f" state, strongly suggesting that the addition of sucrose shifts the "m-to-f" equilibrium toward the "m" state, with no change to the fraction of the "s" state. Furthermore, this modeled behavior for mutants throughout the HNR was confirmed by the acquisition and analysis of EPR spectra for

DOI: 10.1021/bi500894q
Biochemistry 2015, 54, 1717−1728

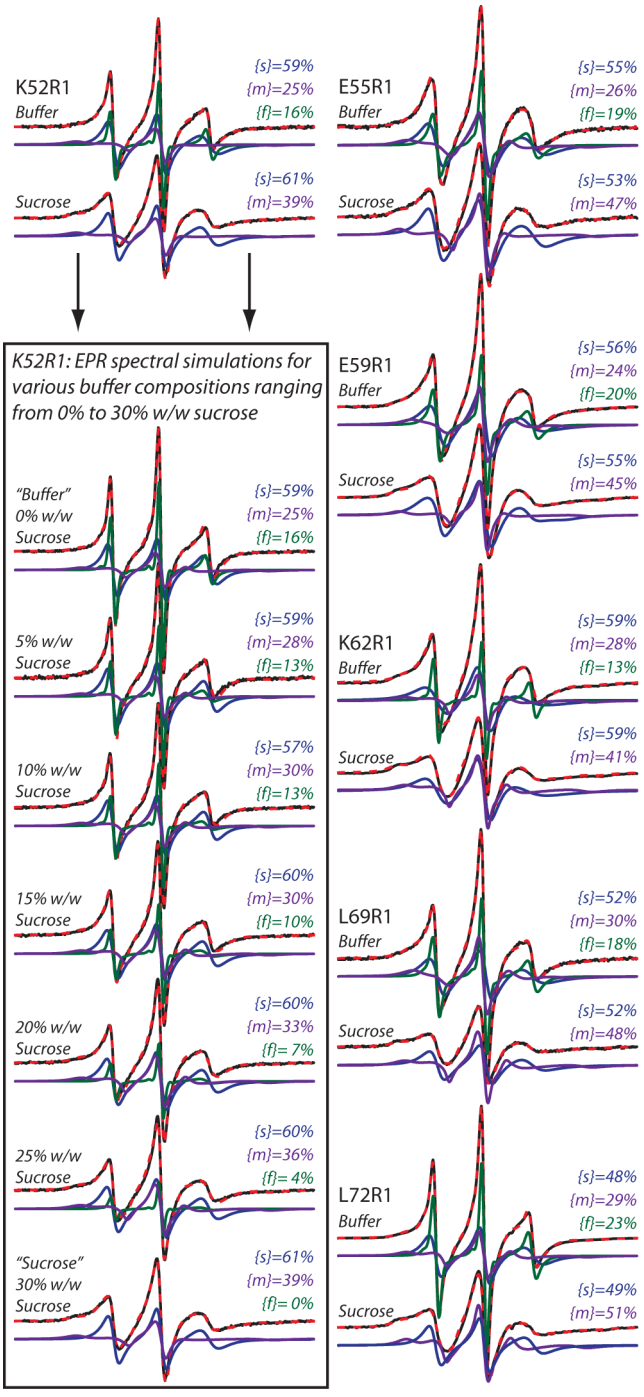

Figure 4. EPR spectra and spectral-fitting simulations for representative spin-labeled stathmin mutants attached to Sepharose: a comparison of line shapes in buffer and 30% w/w sucrose environments. Data (black traces), simulations (red dashed traces), and individual spectral components "s" (blue traces), "m" (purple traces), and "f" (green traces) are presented. For each individual mutant, all dynamic parameters used for the "s" and "m" components except for τ_R were essentially identical between the buffer and sucrose environments (see Tables S2 and S4 of the Supporting Information). Figure S7 presents an equivalent comparison for 16 mutants in and around the HNR in these two environments. Note that the population of the high mobility "f" state is shown to decrease, while that of the "m" state increases as the concentration of sucrose is increased, as is presented with the 0% to 30% w/w sucrose spectral series for the K52R1 mutant (boxed). Similar results are shown for three other stathmin mutants in the HNR in Figure S8. All scans are 100 G wide.

four Sepharose-attached stathmin mutants across a range of sucrose concentrations (see the boxed region of Figure 4 for the spectral series obtained for K52R1, and Figure S8 for equivalent spectral series for the K62R1, A66R1, and L72R1 mutants).

The lack of transition toward the "s" state due to the addition of sucrose (in combination with its slow tumbling rate, high structural heterogeneity, and the nonpolar environment around the spin label deduced from spectral simulation) suggests the interesting possibility that the immobilized state seen in all mutants investigated here may arise from the presence of an oligomeric state of the protein. To explore this possibility we employed complementary techniques of dipolar broadening EPR, native and SDS PAGE, gel filtration chromatography, and static and dynamic light scattering.

Dilution of Spin-Labeled Stathmin Mutants with Wild-Type Protein Results in Sharper Spectral Line Shapes. SDSL-EPR can report the presence of protein oligomers in solution by the technique of wild-type dilution (or "spin dilution") EPR.[51,52] This method depends on the line width broadening effect seen in EPR spectra caused by dipolar coupling between two interacting radical electrons.[20] If a spin-labeled protein forms an ordered oligomer in solution, then two or more nitroxide side chains on neighboring monomer subunits will interact according to an inverse-cubed-radial dependence, resulting in a broadened EPR spectral line width. In practice, this means that two spin labels that are within ~25 Å of one another will exhibit "dipolar-broadened" EPR spectra. Experimentally, for a particular protein that is suspected of oligomerization, this technique involves mixing the spin-labeled protein with its wild-type analogue; as an alternative, instead of wild-type protein, one can use a protein fraction that is spin-labeled with an EPR-inactive side chain (e.g., the acetylated nitroxide labeling reagent 1-acetyl-2,2,5,5-tetramethyl-Δ3-pyrroline-3-methylmethanethiosulfonate), which is also referred to as an "underlabeled" protein.[20] The EPR spectrum recorded for the wild-type diluted mixture will be less broadened than that seen for the pure spin-labeled protein solution; comparison of the relative line widths in the two spectra provides a qualitative indication of oligomerization in the protein.

Two different stathmin mutants, K53R1 and L72R1, were evaluated by the wild-type dilution technique, with the resulting EPR spectral comparisons shown in Figure 5. In these experiments, the protein was immobilized by Sepharose attachment following combination of one part spin-labeled protein to five parts wild-type, and so the resulting oligomers formed are anticipated to exhibit significantly less spectral broadening due to the reduced probability of dipolar coupling in each complex. As expected for the "wild-type diluted" sample spectra seen in Figure 5 (red-dashed traces), we observe sharper lines and a lower intensity downfield shoulder when compared to pure spin-labeled protein spectra (solid black traces). This result strongly indicates reduced dipolar broadening in the wild-type diluted samples.

Complexes Larger than Monomeric Stathmin Are Observed by Native PAGE, SDS PAGE, and Gel Filtration Chromatography. Both native and SDS PAGE experiments were performed for wild-type stathmin solutions with concentrations ranging from 0.68 to 68 mg/mL; representative gels are shown in Figure 6A. It is noted that the concentrations of stathmin used in the EPR experiments above are within this range (~1.7 to 4.2 mg/mL for EPR). The gel obtained under native conditions (Figure 6A, left) reveals a dominant band at an approximate mass of 150 kDa, which is seen across the entire

DOI: 10.1021/bi500894q
Biochemistry 2015, 54, 1717−1728

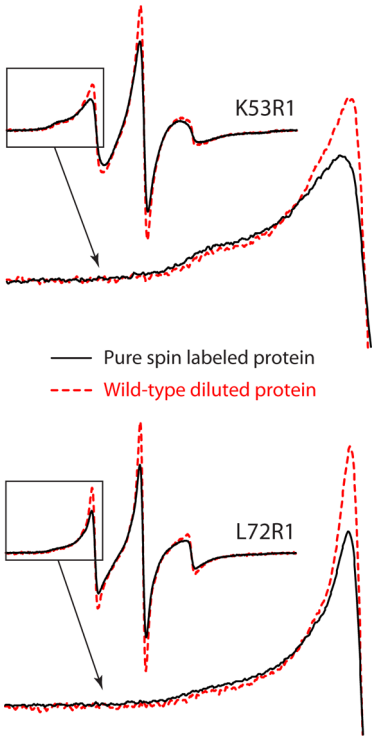

Figure 5. Evaluation of EPR spectral broadening in stathmin oligomers for two different spin-labeled mutants on Sepharose beads in a buffer environment, using the wild-type dilution technique. Broadening of the EPR spectral line shape is compared for solutions of pure spin labeled protein (black solid traces) and of a WT/spin labeled protein mixture ("wild-type diluted" sample, red dashed traces). Spectra recorded for wild-type diluted samples showed significantly sharper line shapes, confirming stathmin oligomerization. The low-field portion of each spectrum is enlarged below each spectrum for clarity. All scans are 100 G wide, integrated areas normalized for direct comparison of lineshapes regardless of relative concentration.

range of concentrations evaluated. Less prominent bands are also present at higher stathmin concentrations, with the smallest mass observed to be just under 20 kDa, in agreement with the 17 kDa mass of monomeric stathmin. Not surprisingly, significant streaking is observed in Lanes 5 and 6 (34 and 68 mg/mL, respectively), indicative of significant aggregation at very high protein concentrations.

The gel obtained after boiling WT stathmin in SDS (Figure 6A, right) is perhaps more worthy of note since, while a band representative of monomeric stathmin is observed across all concentrations, there is a concentration-dependent increase of bands with molecular weights corresponding to dimeric, trimeric, tetrameric, and hexameric stathmin (the darkest of these oligomeric bands are seen at ~65 and ~100 kDa, closest to the expected masses of tetrameric and hexameric stathmin).

Stathmin solutions similar to the lowest concentration samples used in our polyacrylamide gel studies (0.7 and 1.5 mg/mL) were also subjected to gel filtration chromatography (Figure 6B). The gel filtration profiles reveal the presence of small peaks or peak shoulders preceding and following the main peak at ~13.9 mL. While the dominant peak in the chromatogram appears to report a stathmin complex of mass ~65 kDa (corresponding to a tetramer), it is important to mention that the apparent molecular weight of this peak may be attributed to monomeric stathmin in an extended conformation. In fact, Tompa et al. have suggested that the observation of unusually large apparent masses is a hallmark of IDP behavior in size exclusion chromatography.[53,54] In the absence of this phenomenon, we are tempted to identify the very small peak at an elution volume of ~19.9 mL (indicated by the asterisk) as monomeric stathmin,; however, we cannot be wholly certain of its origins. Despite this uncertainty, multimeric complexes are still evident in the sample, with apparent masses ranging from ~150 to 250 kDa, suggesting that, even at the lowest stathmin concentration investigated, the samples are polydisperse due to the presence of higher order oligomers. Taken together, the PAGE and gel filtration profiles for the WT protein suggest that stathmin natively adopts an oligomeric state in solution.

Static and Dynamic Light Scattering Reveal Large Complexes and High Polydispersity in Stathmin Solutions. To further characterize the species present in stathmin solutions, multiangle light scattering (for 0.1−0.3 mg/mL solutions) and dynamic light scattering (for 0.7−1.5 mg/mL solutions) measurements were performed, with the results summarized in Table 2. Despite the low concentrations of the stathmin solutions measured by MALS, very large values for the weight-averaged molecular weights, M_w, were recorded. The average particle masses ranging from ca. 450 to 1000 kDa, hypothetically representative of ~25- to 60-mer complexes, undoubtedly signify skewed results owing to the nature of the static light scattering technique. Namely, because MALS reports a weight-average molecular weight (i.e., not a number-average molecular weight) for all particles in the solution, the presence of trace aggregates or very large oligomers in polydisperse solutions will result in an apparent M_w value shifted toward the mass of the largest particle present in the solution. On the basis of the high degree of polydispersity observed for stathmin solutions in our gel filtration and PAGE experiments, it is not surprising that the M_w value reported by MALS is quite large. Despite filtering each solution through 0.020 μm membranes immediately prior to measurement, it is again apparent that solutions of stathmin protein are neither monodisperse nor monomeric.

Polydisperse, oligomeric stathmin solutions were also indicated by the DLS technique (Table 2 and Figure 6C), as particles with large average hydrodynamic radii ranging from 1.9 to 2.4 nm were observed. The polydispersity values given in Table 2 reflect the width for a particular peak in the particle size distribution plots (Figure 6C); the wider peaks seen for the 1.0 and 1.5 mg/mL solutions in the figure indicate a higher solution polydispersity, and here represent a larger distribution of various oligomers. Note that for each solution measured by DLS, a trace peak of much larger particle size (70−145 nm radius) was also observed. This extra peak accounted for less than 0.3% by mass of the total particles detected in every case and was therefore omitted from Table 2.

A Model of Structural Origins of the Spectral Components Seen in the HNR Region of Spin-Labeled Stathmin. To simplify quantitative spectral analysis, much of the EPR data reported herein are for stathmin immobilized on Sepharose. However, significant commonalities are seen between the spectral simulation parameters for solution-phase and Sepharose-attached samples; in particular, multiple structural states are observed in both environments. On the basis of our EPR simulations of data obtained, it is evident that the HNR of stathmin exists in conformational exchange between two or more structural states at room temperature, which is consistent with the rapid exchange reported by Steinmetz by NMR.[14] The time scale of the EPR experiments allowed us to identify the number of states in exchange and the dynamic features of each state. One

DOI: 10.1021/bi500894q
Biochemistry 2015, 54, 1717−1728

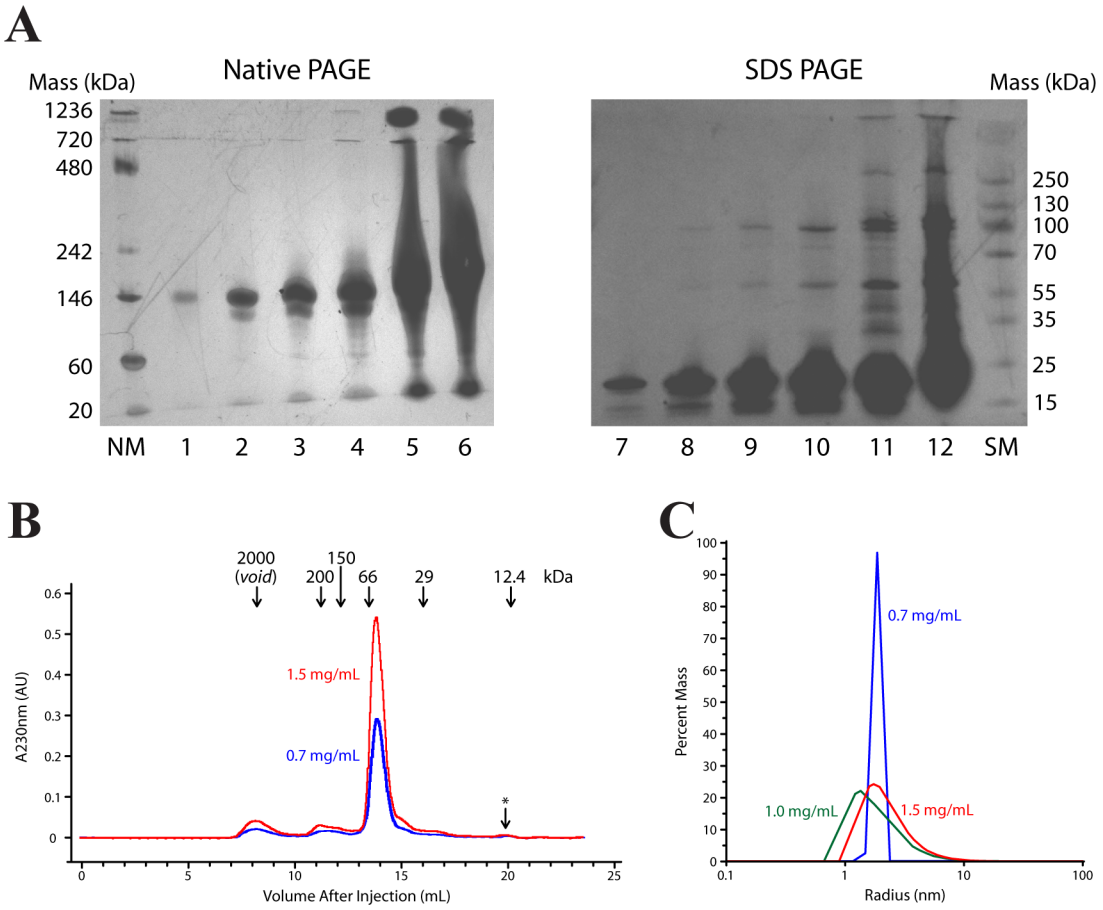

Figure 6. A multiple-technique exploration of stathmin as an oligomer. (A) Native and SDS PAGE separation for wild-type stathmin as a function of concentration. Lane assignments for the native gel (left) are as follows: Lane NM, native marker; Lane 1, 0.68 mg/mL; Lane 2, 1.36 mg/mL; Lane 3, 3.4 mg/mL; Lane 4, 6.8 mg/mL; Lane 5, 34 mg/mL; Lane 6, 68 mg/mL. For the SDS gel (right): Lane 7, 0.68 mg/mL; Lane 8, 1.36 mg/mL; Lane 9, 3.4 mg/mL; Lane 10, 6.8 mg/mL; Lane 11, 17 mg/mL; Lane 12, 34 mg/mL; Lane SM, SDS marker. (B) Gel filtration elution profile of wild-type stathmin at 0.7 (blue trace) and 1.5 mg/mL (red trace). Arrows indicate the elution position of MW markers. Note the dominant peak at around 65 kDa. The first peak (at an elution volume of ~8 mL) corresponds to stathmin aggregates eluted with the column void volume. (C) Particle size distributions of stathmin at 0.7 (blue trace), 1.0 (green trace), and 1.5 mg/mL (red trace) as measured by dynamic light scattering; results indicate nonmonomeric particle sizes and solution polydispersity.

Table 2. Concentration-Dependent Weight-Average Molecular Weights, Average Particle Radii, and Polydispersity Values Recorded for Stathmin Solutions by Multi-Angle and Dynamic Light Scattering[a]

	[stathmin] (mg/mL)	M_w[b] (kDa)
By MALS:	0.1	447(11)
	0.2	634(4)
	0.3	983(13)
	[stathmin] (mg/mL)	<R>[c] (nm)	% polydispersity
By DLS:	0.7	1.9(0.3)	3(3)
	1.0	2.0(0.2)	76(11)
	1.5	2.4(0.1)	61(2)

[a]Values represent weighted averages from replicate measurements; standard deviations are given in parentheses. [b]M_w is the weight-average molecular weight obtained by MALS; for a polydisperse solution this value is significantly shifted toward the mass of the largest particle. [c]<R> is the average hydrodynamic radius of the dominant particle-size peak as reported by DLS.

of the states ("f") exhibits relatively high mobility and a polar environment, and could correspond to an unfolded conformation or a helical state with large backbone fluctuational amplitude. This fast state is highly sensitive to osmolytic perturbation (Figure 4). Another spectral component ("m") reports moderate nitroxide side-chain motion, a nonzero ordering potential, and a polar local environment, which could be representative of a stable helical state. Finally, the largest population state ("s") appears to be structurally heterogeneous, in a nonpolar environment, and insensitive to osmotic perturbation, which we suggest correspond to an oligomer or aggregate state of stathmin. Indeed, the presence of oligomeric species is confirmed in this study by data from the complementary techniques used. Here we propose a model to describe the conformational equilibrium of stathmin in solution and when tethered to Sepharose, which we believe to be consistent with the salient features of the multiple experiments discussed above. As is diagrammed in Figure 7, stathmin in the solution-phase is in conformational exchange between three different states: a highly mobile random coil ("f"), a properly folded helical HNR state ("m"), and a considerably immobilized, dominant state of oligomeric stathmin ("s"). As the molecule tumbles freely in solution, all three stathmin states exhibit spectral diffusion in EPR, which causes the "s" and "m" component line shapes to merge. The highly disordered "f" state tumbles so rapidly that it exhibits its own very sharp and

DOI: 10.1021/bi500894q
Biochemistry 2015, 54, 1717−1728

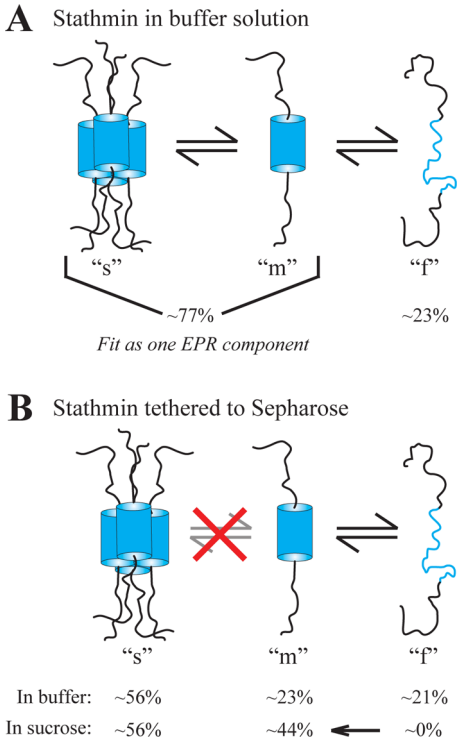

Figure 7. Proposed model for the conformational equilibria that exist for solution-phase and Sepharose-attached stathmin resulting from the analyses of all data presented herein, with approximate populations indicated in percent. (A) In the solution phase, a population equilibrium is established between oligomerized ("s"), folded monomer ("m"), and unfolded monomer ("f") states. In solution, the rapidly tumbling, ordered "s" and "m" states experience rotational diffusion, resulting in merged spectral line shapes (which are difficult to distinguish by X-band CW EPR). The highly disordered "f" state tumbles far more rapidly, exhibiting a separable sharp line shape. (B) Following covalent attachment of stathmin to Sepharose, the monomer-to-oligomer equilibrium is frozen, while the monomer folding transition can still occur. Addition of the osmolyte sucrose drives the helical folding of stathmin, which depopulates the "f" state but does not alter the relative population of the oligomerized state due to immobilization on Sepharose.

distinguishable line shape. Covalent attachment of stathmin to Sepharose acts to "freeze" the monomer-to-oligomer equilibrium, while the coil-to-helix folding transition in individual monomers is still permitted and can now be distinguished. Sucrose preferentially hydrates the stathmin monomer, driving the helical folding of stathmin and depopulating the "f" state (completely so at a concentration of 30% w/w sucrose), even while immobilized on the solid support.

While our model agrees with the assertion of Steinmetz et al. that the HNR of soluble stathmin can populate a folded state in rapid exchange with a disordered state,[12,14] we show here that stathmin can also populate an oligomeric state in solution. We believe that this is the most significant revelation in our examination of stathmin, which is in agreement with the prediction of Doye et al. that stathmin acquires a coiled-coil oligomeric structure due to a heptad repeat sequence found throughout the HNR.[13]

SUMMARY AND FUTURE DIRECTIONS

Using the technique of SDSL-EPR, which is capable of identifying individual protein states with nanosecond or longer lifetimes, we were able to identify and characterize multiple equilibrium states throughout the HNR of stathmin under physiological conditions. Because of the high flexibility and relatively fast tumbling of the intrinsically disordered stathmin protein in solution, separation and characterization of the different dynamic states of the protein by EPR spectroscopy required its covalent attachment to a Sepharose solid support, which aided us in our observation of three or more differentiable protein states. We observed a simple monomer of the protein in an apparent helix–coil equilibrium, but we also identified a structurally heterogeneous and dipolar-broadened state suspected to be a stathmin oligomer. The propensity of stathmin to form a stable oligomer was then confirmed by a number of different techniques, which unequivocally indicated that oligomeric stathmin is, in fact, highly populated in solution. While it is clear that protein immobilization on Sepharose beads has the potential to situate the protein in environments that are biologically unnatural (i.e., locally crowded through tethering via one or more lysine side chains, possibly impacting native conformational exchange behavior), revealed here is its utility in the spectroscopic isolation and identification of the dynamic behaviors and populations of different protein states that are interconnected via solution-phase equilibria.

This result has important implications for our understanding of the equilibrium structures and dynamics of intrinsically disordered proteins in the absence of their binding partners. Namely, the oligomerization of IDPs in the crowded cellular environment may protect them from aggregation or cellular proteolysis, through their stabilization and the creation of an ad hoc hydrophobic core. While such oligomerization has been identified and thoroughly studied in a few different IDPs,[55−60] this behavior could be a conserved phenomenon throughout the class of proteins.

The oligomeric state of stathmin will be explored further in a future publication, where the time scale of the monomer–oligomer equilibrium, reversible aggregation, and tunable oligomerization behavior of the soluble protein will be probed using the spectroscopic techniques of high-pressure CW EPR[61] and pulsed saturation recovery.[62]

ASSOCIATED CONTENT

Supporting Information

Complete EPR spectral data sets, spectral simulations (fits), and tabulated simulation results are provided for the following mutants: nine K-to-A stathmin mutants on Sepharose in a buffer environment, nine K-to-A stathmin mutants in solution in a 30% w/w sucrose environment, 25 spin-labeled stathmin mutants for sites in and around the HNR on Sepharose in a buffer environment, 25 spin-labeled stathmin mutants for sites in and around the HNR in solution in a buffer environment, 16 spin-labeled mutants for sites in and around the HNR on Sepharose in a 30% w/w sucrose environment, and 4 sucrose-dependent spectral series are given in the Supporting Information. Also given are experimental materials and methods for circular dichroism spectroscopy, EPR spectral simulations, native and SDS PAGE, gel filtration chromatography, and multiangle and dynamic light scattering. This material is available free of charge via the Internet at http://pubs.acs.org.

AUTHOR INFORMATION

Corresponding Author

*E-mail: mibridges@fullerton.edu. Phone: (657) 278-2276.

DOI: 10.1021/bi500894q
Biochemistry 2015, 54, 1717−1728

Author Contributions

[§]A.J.C., C.J.L., and M.D.B. contributed equally to this work.

Funding

This research was supported by an award from Research Corporation for Science Advancement (CCSA#20907 - MDB) and the California State University Fullerton Research Incentive Award.

Notes

The authors declare no competing financial interest.

■ ACKNOWLEDGMENTS

We are grateful to Wayne Hubbell and Christian Altenbach for their helpful lessons on the general EPR spectral fitting technique, and Dr. Joseph Horowitz for technical assistance in use of the CD spectrometer. We thank Stephanie Borja and Jesus Mejia for their thoughtful comments on the manuscript.

■ ABBREVIATIONS

CW, continuous wave; EPR, electron paramagnetic resonance; "f", fast, high mobility dynamic component; far-UV CD, far-ultraviolet circular dichroism; DLS, dynamic light scattering; HNR, helical nucleation region; IDP, intrinsically disordered protein; K-to-A, lysine to alanine mutant; "m", moderate mobility dynamic component; MALS, multiangle light scattering; MBP, maltose binding protein; MOMD, microscopic order macroscopic disorder model; MTSSL, methanethiosulfonate spin label; NLSL, nonlinear least-squares stochastic Liouville program; NMR, nuclear magnetic resonance; PAGE, polyacrylamide gel electrophoresis; "s", slow, low mobility dynamic component; R1, nitroxide spin label as a protein side chain; SDS, sodium dodecyl sulfate; SDSL, site-directed spin-labeling; TEV, tobacco etch virus; WT, wild-type

■ REFERENCES

(1) Ward, J. J., Sodhi, J. S., McGuffin, L. J., Buxton, B. F., and Jones, D. T. (2004) Prediction and functional analysis of native disorder in proteins from the three kingdoms of life. *J. Mol. Biol. 337*, 635−645.

(2) Oldfield, C. J., Cheng, Y., Cortese, M. S., Brown, C. J., Uversky, V. N., and Dunker, A. K. (2005) Comparing and combining predictors of mostly disordered proteins. *Biochemistry 44*, 1989−2000.

(3) Dunker, A. K., Oldfield, C. J., Meng, J., Romero, P., Yang, J. Y., Chen, J. W., Vacic, V., Obradovic, Z., and Uversky, V. N. (2008) The unfoldomics decade: an update on intrinsically disordered proteins. *BMC Genomics 9* (Suppl 2), S1.

(4) Wright, P. E., and Dyson, H. J. (2009) Linking folding and binding. *Curr. Opin. Struct. Biol. 19*, 31−38.

(5) Fink, A. L. (2005) Natively unfolded proteins. *Curr. Opin. Struct. Biol. 15*, 35−41.

(6) Dunker, A. K., Silman, I., Uversky, V. N., and Sussman, J. L. (2008) Function and structure of inherently disordered proteins. *Curr. Opin. Struct. Biol. 18*, 756−764.

(7) Henzler-Wildman, K., and Kern, D. (2007) Dynamic personalities of proteins. *Nature 450*, 964−972.

(8) Frieden, C. (2007) Protein aggregation processes: In search of the mechanism. *Protein Sci. 16*, 2334−2344.

(9) Zerovnik, E. (2011) Oligomerization preceding amyloid fibril formation: a process in common to intrinsically disordered and globular proteins. *Network 22*, 154−161.

(10) Baldassarre, G., Belletti, B., Nicoloso, M. S., Schiappacassi, M., Vecchione, A., Spessotto, P., Morrione, A., Canzonieri, V., and Colombatti, A. (2005) p27(Kip1)−stathmin interaction influences sarcoma cell migration and invasion. *Cancer Cell 7*, 51−63.

(11) Honnappa, S., Cutting, B., Jahnke, W., Seelig, J., and Steinmetz, M. O. (2003) Thermodynamics of the Op18/stathmin-tubulin interaction. *J. Biol. Chem. 278*, 38926−38934.

(12) Steinmetz, M. O. (2007) Structure and thermodynamics of the tubulin-stathmin interaction. *J. Struct. Biol. 158*, 137−147.

(13) Doye, V., Soubrier, F., Bauw, G., Boutterin, M. C., Beretta, L., Koppel, J., Vandekerckhove, J., and Sobel, A. (1989) A single cDNA encodes two isoforms of stathmin, a developmentally regulated neuron-enriched phosphoprotein. *J. Biol. Chem. 264*, 12134−12137.

(14) Steinmetz, M. O., Kammerer, R. A., Jahnke, W., Goldie, K. N., Lustig, A., and van Oostrum, J. (2000) Op18/stathmin caps a kinked protofilament-like tubulin tetramer. *EMBO J. 19*, 572−580.

(15) Molina-Garcia, A. D. (1999) Hydrostatic pressure in ultracentrifugation (revisited). *Prog. Colloid Polym. Sci. 113*, 57−61.

(16) Ariesandi, W., Chang, C.-F., Chen, T.-E., and Chen, Y. R. (2013) Temperature-dependent structural changes of Parkinson's alpha-synuclein reveal the role of pre-existing oligomers in alpha-synuclein fibrillization. *PLoS One 8*, e53487.

(17) Mchaourab, H. S., Lietzow, M. A., Hideg, K., and Hubbell, W. L. (1996) Motion of spin-labeled side chains in T4 lysozyme. Correlation with protein structure and dynamics. *Biochemistry 35*, 7692−7704.

(18) Columbus, L., and Hubbell, W. L. (2002) A new spin on protein dynamics. *Trends Biochem. Sci. 27*, 288−295.

(19) Columbus, L., and Hubbell, W. L. (2004) Mapping backbone dynamics in solution with site-directed spin-labeling: GCN4−58 bZip free and bound to DNA. *Biochemistry 43*, 7273−7287.

(20) Altenbach, C., Oh, K.-J., Trabanino, R., Hideg, K., and Hubbell, W. L. (2001) Estimation of inter-residue distances in spin labeled proteins at physiological temperatures: experimental strategies and practical limitations. *Biochemistry 40*, 15471−15482.

(21) Drescher, M. (2012) EPR in protein science: intrinsically disordered proteins. *Top. Curr. Chem. 321*, 91−119.

(22) Drescher, M., Godschalk, F., Veldhuis, G., van Rooijen, B. D., Subramaniam, V., and Huber, M. (2008) Spin-label EPR on alpha-synuclein reveals differences in the membrane binding affinity of the two antiparallel helices. *ChemBiochem 9*, 2411−2416.

(23) Chen, M., Margittai, M., Chen, J., and Langen, R. (2007) Investigation of alpha-synuclein fibril structure by site-directed spin-labeling. *J. Biol. Chem. 282*, 24970−24979.

(24) Torok, M., Milton, S., Kayed, R., Wu, P., McIntire, T., Glabe, C. G., and Langen, R. (2002) Structural and dynamic features of Alzheimer's Abeta peptide in amyloid fibrils studied by site-directed spin-labeling. *J. Biol. Chem. 277*, 40810−40815.

(25) Murakami, K., Hara, H., Masuda, Y., Ohigashi, H., and Irie, K. (2007) Distance measurement between Tyr10 and Met35 in amyloid beta by site-directed spin-labeling ESR spectroscopy: implications for the stronger neurotoxicity of Abeta42 than Abeta40. *ChemBiochem 8*, 2308−2314.

(26) Sepkhanova, I., Drescher, M., Meeuwenoord, N. J., Limpens, R. W., Koning, R. I., Filippov, D. V., and Huber, M. (2009) Monitoring Alzheimer amyloid peptide aggregation by EPR. *Appl. Magn. Reson. 36*, 209−222.

(27) Lundberg, K. M., Stenland, C. J., Cohen, F. E., Prusiner, S. B., and Millhauser, G. L. (1997) Kinetics and mechanism of amyloid formation by the prion protein H1 peptide as determined by time dependent ESR. *Chem. Biol. 4*, 345−355.

(28) Igarashi, R., Sakai, T., Hara, H., Tenno, T., Tanaka, T., Tochio, H., and Shirakawa, M. (2010) Distance determination in proteins inside Xenopus laevis oocytes by double electron-electron resonance experiments. *J. Am. Chem. Soc. 132*, 8228−8229.

(29) Morin, B., Bourhis, J. M., Belle, V., Woudstra, M., Carriere, F., Guigliarelli, B., Fournel, A., and Longhi, S. (2006) Assessing induced folding of an intrinsically disordered protein by site-directed spin-labeling electron paramagnetic resonance spectroscopy. *J. Phys. Chem. B 110*, 20596−20608.

(30) Laganowsky, A., Benesch, J. L., Landau, M., Ding, L., Sawaya, M. R., Cascio, D., Huang, Q., Robinson, C. V., Horowitz, J., and Eisenberg, D. (2010) Crystal structures of truncated alphaA and alphaB crystallins reveal structural mechanisms of polydispersity important for eye lens function. *Protein Sci. 19*, 1031−1043.

(31) Leitzow, M. A., and Hubbell, W. L. (2004) Motion of spin label side chains in cellular retinol-binding protein: correlation with structure

DOI: 10.1021/bi500894q
Biochemistry 2015, 54, 1717−1728

and nearest-neighbor interactions in an antiparallel β-sheet. *Biochemistry 43*, 3137−3151.
(32) Fleissner, M. R., Cascio, D., and Hubbell, W. L. (2009) Structural origins of weakly ordered motion in spin-labeled proteins. *Protein Sci. 18*, 893−908.
(33) Columbus, L., Kálai, T., Jeko, J., Hideg, K., and Hubbell, W. L. (2001) Molecular motion of spin-labeled side chains in alpha-helices: analysis by variation of side chain structure. *Biochemistry 40*, 3828−3846.
(34) Altenbach, C. Multicomponent, version 761; LabVIEW programs for the analysis of EPR Data. https://sites.google.com/site/altenbach/labview-programs/epr-programs/ (accessed July 19, 2014).
(35) Budil, D. E., Lee, S., Saxena, S., and Freed, J. H. (1996) Nonlinear-least-squares analysis of slow-motion EPR spectra in one and two dimensions using a modified Levenberg-Marquard algorithm. *J. Magn. Reson. Ser. A 120*, 155−189.
(36) Hubbell, W. L., Cafiso, D. S., and Altenbach, C. (2000) Identifying conformational changes with site-directed spin-labeling. *Nat. Struct. Mol. Biol. 7*, 735−739.
(37) Hubbell, W. L., Gross, A., Langen, R., and Lietzow, M. A. (1998) Recent advances in site-directed spin-labeling of proteins. *Curr. Opin. Struct. Biol. 8*, 649−656.
(38) Hubbell, W. L., López, C. J., Altenbach, C., and Yang, Z. (2013) Technological advances in site-directed spin-labeling of proteins. *Curr. Opin. Struct. Biol. 23*, 725−733.
(39) Guo, Z., Cascio, D., Hideg, K., Kálai, T., and Hubbell, W. L. (2007) Structural determinants of nitroxide motion in spin-labeled proteins: Tertiary contact and solvent-inaccessible sites in helix G of T4 lysozyme. *Protein Sci. 16*, 1069−1086.
(40) Guo, Z., Casio, D., Hideg, K., and Hubbell, W. L. (2008) Structural determinants of nitroxide motion in spin-labeled proteins: Solvent-exposed sites in helix B of T4 lysozyme. *Protein Sci. 17*, 228−239.
(41) López, C. J., Fleissner, M. R., Guo, Z., Kusnetzow, A. K., and Hubbell, W. L. (2009) Osmolyte perturbation reveals conformational equilibria in spin-labeled proteins. *Protein Sci. 18*, 1637−1652.
(42) Yang, Z., Liu, Y., Borbat, P., Zweier, J. L., Freed, J. H., and Hubbell, W. L. (2012) Pulsed ESR dipolar spectroscopy for distance measurements in immobilized spin-labeled proteins in liquid solution. *J. Am. Chem. Soc. 134*, 9950−9952.
(43) López, C. J., Fleissner, M. R., Brooks, E. K., and Hubbell, W. L. (2014) Stationary-phase EPR for exploring protein structure, conformation, and dynamics in spin-labeled proteins. *Biochemistry 53*, 7067−7075.
(44) Fleissner, M. R., Bridges, M. D., Brooks, E. K., Cascio, D., Kálai, T., Hideg, K., and Hubbell, W. L. (2011) Structure and dynamics of a conformationally constrained nitroxide side chain and applications in EPR spectroscopy. *Proc. Natl. Acad. Sci. U.S.A. 108*, 16241−16246.
(45) Arakawa, T., and Timasheff, S. N. (1985) The stabilization of proteins by osmolytes. *Biophys. J. 47*, 411−414.
(46) Auton, M., Ferreon, A. C., and Bolen, D. W. (2006) Metrics that differentiate the origins of osmolyte effects on protein stability: a test of the surface tension proposal. *J. Mol. Biol. 361*, 983−992.
(47) Uversky, V. (2009) Intrinsically disordered proteins and their environment: effects of strong denaturants, temperature, pH, counter ions, membranes, binding partners, osmolytes, and macromolecular crowding. *Protein J. 28*, 305−325.
(48) Macchi, F., Eisenkolb, M., Kiefer, H., and Otzen, D. E. (2012) The effect of osmolytes on protein fibrillation. *Int. J. Mol. Sci. 13*, 3801−3819.
(49) Mokdad, A., Herrick, D. Z., Kahn, A. K., Andrews, E., Kim, M., and Cafiso, D. S. (2012) Ligand-induced structural changes in the *Escherichia coli* ferric citrate transporter reveal modes for regulating protein-protein interactions. *J. Mol. Biol. 423*, 818−830.
(50) Fleissner, M. R., Brustad, E. M., Kálai, T., Altenbach, C., Cascio, D., Peters, F. B., Hideg, K., Peuker, S., Schultz, P. G., and Hubbell, W. L. (2009) Site-directed spin-labeling of a genetically encoded unnatural amino acid. *Proc. Natl. Acad. Sci. U.S.A. 106*, 21637−21642.
(51) Berengian, A. R., Parfenova, M., and Mchaourab, H. S. (1999) Site-directed spin labeling study of subunit interactions in the α-Crystallin domain of small heat-shock proteins: Comparison of the oligomer symmetry in αA-Crystallin, HSP 27, and HSP 16.3. *J. Biol. Chem. 274*, 6305−6314.
(52) Stone, K. M., Voska, J., Kinnebrew, M., Pavlova, A., Junk, M. J. N., and Han, S. (2013) Structural insight into proteorhodopsin oligomers. *Biophys. J. 104*, 472−481.
(53) Csizmók, V., Szollosi, E., Friedrich, P., and Tompa, P. (2006) A novel two-dimensional electrophoresis technique for the identification of intrinsically unstructured proteins. *Mol. Cell. Proteomics 5*, 265−273.
(54) Tantos, A., Szrnka, K., Szabo, B., Bokor, M., Kamasa, P., Matus, P., Bekesi, A., Tompa, K., Han, K. H., and Tompa, P. (2013) Structural disorder and local order of hNopp140. *Biochim. Biophys. Acta 1834*, 342−350.
(55) Wan, O. W., and Chung, K. K. (2012) The role of alpha-synuclein oligomerization and aggregation in cellular and animal models of Parkinson's disease. *PLoS One 7*, e38545.
(56) Fredenburg, R. A., Rospigliosi, C., Meray, R. K., Kessler, J. C., Lashuel, H. A., Eliezer, D., and Lansbury, P. T. (2007) The impact of the E46K mutation on the properties of alpha-synuclein in its monomeric and oligomeric states. *Biochemistry 46*, 7107−7118.
(57) Winner, B., Jappelli, R., Maji, S. K., Desplats, P. A., Boyer, L., Aigner, S., Hetzer, C., Loher, T., Vilar, M., Campioni, S., Tzitzilonis, C., Soragni, A., Jessberger, S., Mira, H., Consiglio, A., Pham, E., Masliah, E., Gage, F. H., and Riek, R. (2011) In vivo demonstration that alpha-synuclein oligomers are toxic. *Proc. Natl. Acad. Sci. U.S.A. 108*, 4194−4199.
(58) Lesné, S. E., Sherman, M. A., Grant, M., Kuskowski, M., Schneider, J. A., Bennett, D. A., and Ashe, K. H. (2013) Brain amyloid-β oligomers in ageing and Alzheimer's disease. *Brain 136*, 1383−1398.
(59) Haass, C., and Selkoe, D. J. (2007) Soluble protein oligomers in neurodegeneration: lessons from the Alzheimer's amyloid beta-peptide. *Nat. Rev. Mol. Cell. Biol. 8*, 101−112.
(60) Perevozchikova, T., Stanley, C. B., McWilliams-Koeppen, H. P., Rowe, E. L., and Berthelier, V. (2014) Investigating the structural impact of the glutamine repeat in huntingtin assembly. *Biophys. J. 107*, 411−421.
(61) McCoy, J., and Hubbell, W. L. (2011) High pressure EPR reveals conformational equilibria and compressibility changes in spin labeled proteins. *Proc. Natl. Acad. Sci. U. S. A. 108*, 1331−1336.
(62) Bridges, M. D., Hideg, K., and Hubbell, W. L. (2010) Resolving conformational and rotameric exchange in spin-labeled proteins using saturation recovery EPR. *Appl. Magn. Reson. 37*, 363−390.

DOI: 10.1021/bi500894q
Biochemistry 2015, 54, 1717−1728